Pressure and alloying effects on the metal to insulator transition in $NiS_{2-x}Se_x$ studied by infrared spectroscopy

A. Perucchi,[1,2] C. Marini,[2] M. Valentini,[2] P. Postorino,[2] R. Sopracase,[2] P. Dore,[2] P. Hansmann,[3,4] O. Jepsen,[3] G. Sangiovanni,[3,4] A. Toschi,[3,4] K. Held,[4] D. Topwal,[5] D. D. Sarma,[6,7] and S. Lupi[2]

[1]*Sincrotrone Trieste S.C.p.A., Area Science Park, I-34012 Basovizza, Trieste, Italy*

[2]*CNR-INFM COHERENTIA and Dipartimento di Fisica, Università di Roma "La Sapienza," Piazzale Aldo Moro 2, I-00185 Roma, Italy*

[3]*Max-Planck Institut für Festkörperforschung, Heisenbergstrasse 1, D-70569 Stuttgart, Germany*

[4]*Institute for Solid State Physics, Vienna University of Technology, 1040 Wien, Austria*

[5]*International Centre for Theoretical Physics (ICTP), Strada Costiera 11, 34100 Trieste, Italy*

[6]*Centre for Advanced Materials, Indian Association for the Cultivation of Science, Jadarpur, Kolkata 70032, India*

[7]*Solid State and Structural Chemistry Unit, Indian Institute of Science, Bangalore 560012, India*

(Received 1 July 2009; published 6 August 2009)

The metal to insulator transition in the charge-transfer $NiS_{2-x}Se_x$ compound has been investigated through infrared reflectivity. Measurements performed by applying pressure to pure NiS_2 (lattice contraction) and by Se alloying (lattice expansion) reveal that in both cases an anomalous metallic state is obtained. We find that optical results are not compatible with the linear Se-alloying vs pressure-scaling relation previously established through transport, thus pointing out the substantially different microscopic origin of the two transitions.

DOI: 10.1103/PhysRevB.80.073101 PACS number(s): 71.30.+h, 62.50.−p, 78.30.−j

Understanding the physics of strongly correlated systems is one of the most challenging tasks of condensed-matter research.[1] Besides displaying extremely interesting physical behavior, their sensitivity to small changes in external parameters makes them highly appealing for future technological applications. That sensitivity is attributed to the small value of the electron bandwidth in comparison with other relevant energy scales as the electron correlation U or the charge-transfer (CT) energy gap. The independent electron approximation breaks down and materials at half filling can be insulators, contrary to the prediction of band theory.

The cubic pyrite NiS_2, which is a CT insulator following the Zaanen-Sawatsky-Allen classification scheme,[2] is considered, together with vanadium sesquioxide V_2O_3, a textbook example of strongly correlated materials. NiS_2 attracts particular interest as it easily forms a solid solution with $NiSe_2$ ($NiS_{2-x}Se_x$), which, while being isoelectronic and isostructural to NiS_2, is nevertheless a good metal. A metal to insulator transition (MIT), induced by Se alloying, is observed at room temperature (T) for $x \approx 0.6$, and a magnetic phase boundary from an antiferromagnetic to a paramagnetic metal is found at low T at about $x=1$ [see the inset of Fig. 1(a)].[1] An alternative way to induce a metallic state in NiS_2 is applying a hydrostatic pressure (P). Following Mott's original idea,[3] this technically challenging procedure offers the unique opportunity to continuously tune the bandwidth, without introducing impurities or disorder. High-P techniques have indeed been used in the past few years to investigate the dc transport properties of $NiS_{2-x}Se_x$,[4,5] and a P-induced MIT has been observed in pure NiS_2 for $P > 4$ GPa.

Infrared reflectivity, in particular, under pressure, is a very suitable probe to address the physics of strongly correlated systems. The investigation of the T-dependent optical properties of V_2O_3 and their theoretical explanation in terms of coherent and incoherent excitations around the Fermi energy (E_F) represents one of the most compelling successes of the dynamical mean-field theory (DMFT).[6–8] However, with few remarkable exceptions,[9–12] infrared investigations of the MIT in CT insulators are still rare and a thorough optical study of $NiS_{2-x}Se_x$ vs Se alloying and applied P is completely lacking to the best of our knowledge. In this Brief Report we fill this gap, presenting room-T reflectivity measurements over a broad spectral range on four compounds ($x=0$, 0.55, 0.6, and

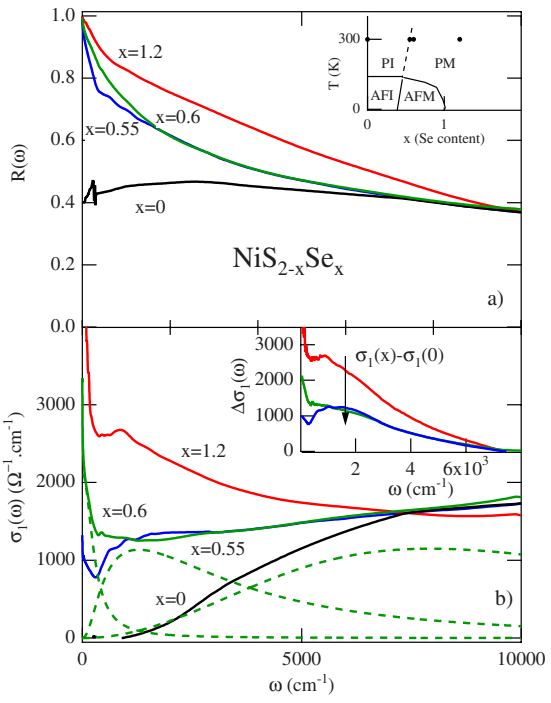

FIG. 1. (Color online) (a) Optical reflectivity of $NiS_{2-x}Se_x$ for $x=0$, 0.55, 0.6, and 1.2 at ambient conditions. Inset: Phase diagram of $NiS_{2-x}Se_x$.[1] Black dots correspond to the samples measured in this work. (b) Optical conductivities from KK transformations. Thick dashed lines represent the DL fit of the $x=0.6$ sample. Inset: Difference $\Delta\sigma_1=\sigma_1(x)-\sigma_1(x=0)$ spectra.

1.2) of the $NiS_{2-x}Se_x$ series together with optical measurements as a function of P on pure NiS_2. Experimental data are compared with local-density approximation (LDA) calculations and the resulting scenario for the two MITs is finally depicted.

The ambient P nearly normal-incidence reflectivity $R(\omega)$ has been measured between 50 and 35 000 cm^{-1} on well characterized high-density pellets of $NiS_{2-x}Se_x$.[13,14] An *in situ* evaporation technique was used to measure the reference. The high-P study has been performed using a diamond-anvil cell (DAC). A small piece of NiS_2 was loaded inside the gasket hole together with KBr as hydrostatic medium. Great care was taken to obtain a clean sample-diamond interface where reflectivity spectra, $R_{sd}(\omega)$, have been measured.[15] The measurement was performed at the high brightness infrared synchrotron-radiation source SISSI@Elettra (Trieste).[16] Further details on the measurement procedures are reported elsewhere.[17,18]

The $R(\omega)$ of NiS_2 at ambient P, shown in Fig. 1(a), is nearly flat from 50 to 10 000 cm^{-1} except for weak phonon contributions at 260 and 290 cm^{-1}. On increasing the Se content, $R(\omega)$ is progressively enhanced at low frequencies, characteristic of a metallic behavior. The real part of the optical conductivity $\sigma_1(\omega)$ [Fig. 1(b)] has been determined through Kramers-Kronig (KK) transformations. To this end, standard extrapolation procedures were adopted at both high and low frequency.[19,20]

The optical conductivity of NiS_2 is strongly depleted at low frequency showing the CT gap (evaluated at full width half maximum of the absorption) at about 4000 cm^{-1}. This is consistent with previous optical measurements[4,21]. On increasing the Se content x, a large amount of spectral weight (SW) is transferred from high to low frequency through an isosbestic point around 8000 cm^{-1}. This suggests the main role played in the MIT by electronic correlations.[1] As it is better highlighted by the $\Delta\sigma_1=\sigma_1(x)-\sigma_1(x=0)$ difference spectra in the inset of Fig. 1(b), the low-energy contribution to the $\sigma_1(\omega)$ is made up of two well distinct terms: one broad mid-IR band peaked around 2000 cm^{-1} and extending up to nearly 8000 cm^{-1}, and a sharp contribution below 500 cm^{-1}. In analogy with spectra of metallic V_2O_3,[6,7] the narrow peak is attributed to quasiparticle (QP) coherent excitations around E_F while the mid-IR term is associated to optical transitions from the QP peak to the upper and lower Hubbard bands. This scenario has been confirmed by fitting the $\sigma_1(\omega)$ curves through a Drude-Lorentz (DL) model. Data can be described by a Drude term plus two Lorentzian oscillators. The Drude and the low-energy oscillator (centered around 2000 cm^{-1}) describe the coherent and the mid-IR excitations around E_F while the remaining oscillator at 10 000 cm^{-1} mimics the CT and Hubbard transitions. The fitting components are reported as thick dashed lines in Fig. 1(b) for $x=0.6$.

We turn now to the high-P measurements on NiS_2. The reflectivity at the sample-diamond interface, $R_{sd}(\omega)$ (thick solid lines), is shown in Fig. 2(a). The strong two-phonon diamond absorption provides reliable data only above 2000 cm^{-1}. On increasing the pressure, $R_{sd}(\omega)$ is progressively enhanced at low frequency showing an overdamped behavior [similarly to $R_{sd}^{cal}(\omega)$ obtained on varying x], as a signature for a correlated bad metallic state. At high frequencies all $R_{sd}(\omega)$ converge above 10 000 cm^{-1}. In order to evaluate the accuracy of our high-P measurements, we compare the $R_{sd}(\omega)$ data to the expected reflectivity at a sample-diamond interface, $R_{sd}^{cal}(\omega)$, calculated by using a procedure previously introduced.[17,18] The calculated $R_{sd}^{cal}(\omega)$ for NiS_2 [dashed lines in Fig. 2(a)] is in good agreement with $R_{sd}(\omega)$ measured in the DAC at the lowest pressure (1.1 GPa) being both nearly flat and with a value ≈20% over the whole frequency range. The same procedure has been applied to $NiS_{2-x}Se_x$ ($x=0.55$, 0.6, and 1.2) compounds and the resulting $R_{sd}^{cal}(\omega)$ are shown in Fig. 2(a) for the sake of comparison. We then tried to fit the $R_{sd}(\omega)$ measured vs P for NiS_2 within the same DL framework previously used for $NiS_{2-x}Se_x$ at ambient P. Although a certain degree of arbitrariness re-

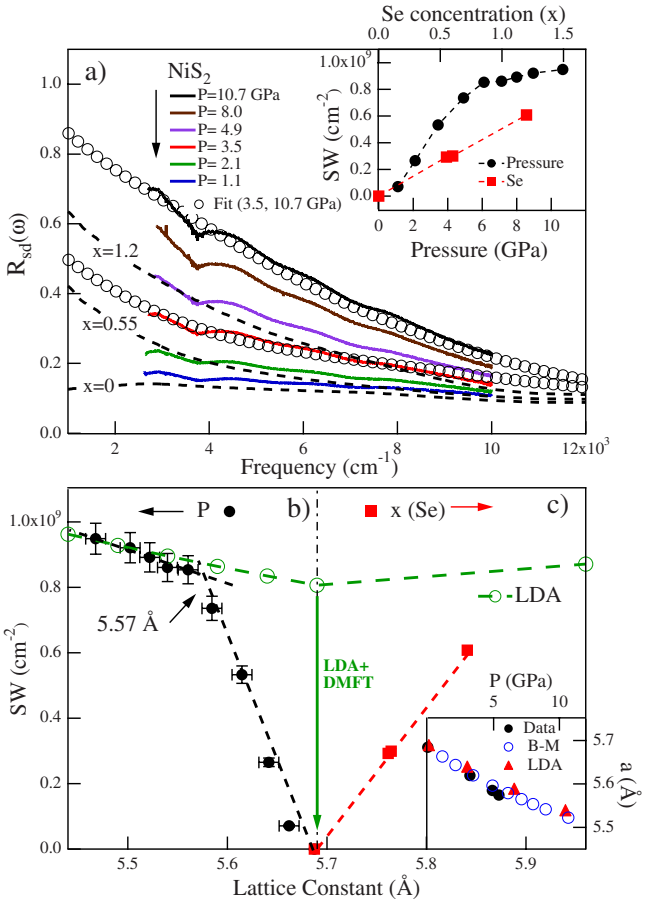

FIG. 2. (Color online) (a) $R_{sd}(\omega)$ measured for NiS_2 at high-P (thick solid lines) (open symbols show DL fits) and calculated $R_{sd}^{cal}(\omega)$ at sample-diamond interface for $NiS_{2-x}Se_x$ at selected x (dashed lines). The kink in $R_{sd}(\omega)$ at about 3700 cm^{-1} is instrumental. Inset: QP spectral weight vs P (bottom) and x (top); top and bottom scales are chosen consistently with a scaling factor $f \approx 0.14/\text{GPa}$ (see text). Lower panels: (b) QP spectral weight (see text) vs lattice constant a for NiS_2 and (c) $NiS_{2-x}Se_x$. Open circles are square plasma frequency values calculated with LDA (see text). A rescaling factor of 1.25 has been used for the comparison with the experimental data. The dashed-dotted vertical line marks the a value for NiS_2 at ambient conditions. Inset: lattice parameter vs P. Experimental data from Ref. 24 (solid circles), calculated values using the B-M equation (open circles) and LDA (solid triangles).

mains in fitting the data over a restricted spectral range, a reliable description of the $R_{sd}(\omega)$ at any P is obtained by the sum of a Drude and a mid-IR term plus a high-frequency oscillator kept constant at all pressures. This fit provides a robust estimate of the quasiparticle SW, defined by the sum of the Drude and of the mid-IR intensities. This sum remains nearly unchanged by varying the fitting parameters over realistic ranges.

The microscopic mechanisms inducing the P and Se MITs are further investigated by studying the quasiparticle SW as a function of the cubic lattice parameter a. The lattice is expanded by Se alloying[22,23] whereas it is compressed by pressure.[24] The x and the P dependence (up to ≈ 5 GPa) of a have been obtained from Refs. 23 and 24, respectively. Data at higher P have been estimated using the procedure developed in Ref. 15. Through the specific-heat results of Ref. 25, which provide a Debye frequency $\omega_D \approx 350$ cm^{-1} well comparable with the NiS_2 phonon frequencies, we obtain a sound velocity $v_s \approx 4300$ m/s. As the density of NiS_2 is $\rho = 4455$ kg/m^3, the Bulk modulus results $B_0 = \rho \times v_s^2 \approx 83$ GPa. Assuming $B(P) = B_0 + B'P$, $a(P)$ is finally given by the Birch-Murnagham (B-M) equation[26]

$$a(P) = a(0) * \left[1 + \frac{B'}{B_0} * P \right]^{-1/3B'}, \qquad (1)$$

where B' normally ranges between 4 and 8.[27] The experimental $a(P)$ data, the values estimated from Eq. (1) and those from LDA calculations[28] are in a very good agreement as shown in the inset of Fig. 2(c).

The quasiparticle SW, shown for pure NiS_2 at working P in Fig. 2(b) and for $NiS_{2-x}Se_x$ at different Se contents in Fig. 2(c), reveals a striking nonmonotonic behavior as a function of a. Its slow continuous increase for $a < 5.57$ Å (i.e., at the highest values of P) reflects the progressive enhancement of the kinetic energy due to the applied P and corresponds to a nearly complete metallization of NiS_2. For $a > 5.57$ Å up to $a_{eq} \approx 5.68$ Å (namely, the lattice parameter corresponding to NiS_2 at ambient conditions), correlation effects get larger and the SW drops rapidly to zero as a consequence of the Mott transition. On further increasing a above a_{eq} due to the Se alloying, the SW [Fig. 2(c)] restarts to increase, owing to the onset of the Se-induced MIT.

Despite the opposite behavior of the lattice parameter vs Se alloying and pressure, a linear scaling factor $f \approx 0.14$/GPa between x and P has been formerly established from low-T dc-resistivity data,[4,5] thus suggesting an equivalency between the two MITs. However, the same f does not apply comparing the optical SW dependence on P and x. It is indeed clear from the inset of Fig. 2(a) that the rate of increase in SW is much larger with P than with x. The breakdown at finite frequencies of the dc linear scaling between x and P suggests that while a metallic state can be obtained from NiS_2 both by applying P and by alloying Se, this state takes place through substantially different microscopic mechanisms, involving different redistributions in the electronic density of states. A qualitative understanding of the two different MITs can be obtained through self-consistent tight-binding linear-muffin tin-orbital (TB-LMTO) LDA calculations,[30] see Fig. 3. To this end, we employed the Nth order muffin-tin orbital (NMTO) downfolding[31] and the augmented plane waves plus local-orbitals (APW+lo) techniques within the framework of the WIEN2K code.[32] At ambient P the Ni e_g states with a bandwidth $W_{e_g} = 2.1$ eV and the antibonding $pp\sigma^*$-S states are separated by a CT gap (Δ_{LDA}) centered around 1.5 eV. Beside this gap, a second LDA-CT gap is present between occupied $pp\pi$-S states below E_F and the e_g-Ni states (see, e.g., Ref. 33). Upon applying pressure, the lattice contracts and the entire band structure around E_F is renormalized, e.g., by a factor of 1.13 at $P = 10$ GPa [dashed curve in Fig. 3(a)]. All features of the density of states (DOS) stay the same, in particular, the energy scales, (W_{e_g} and Δ_{LDA}, are rescaled by a factor 1.13). Hence, the bandwidth-gap ratio W_{e_g}/Δ_{LDA} remains nearly constant. On the other hand, the interaction U can be assumed to be constant so that W_{e_g}/U increases by the factor 1.13, triggering a bandwidth-controlled MIT. In the case of Se substitution, the lattice expands (instead of shrinking) due to the larger atomic radius of Se ions. This leads to a very complementary scenario while the changes in the e_g bandwidth W_{e_g} are negligible, the CT gaps shrink [see Fig. 3(b)]. Assuming U again to be constant, the driving force for the MIT is now the reduction in the charge-transfer gap (W_{e_g}/Δ_{LDA} increases, as W_{e_g} remains basically unaffected).

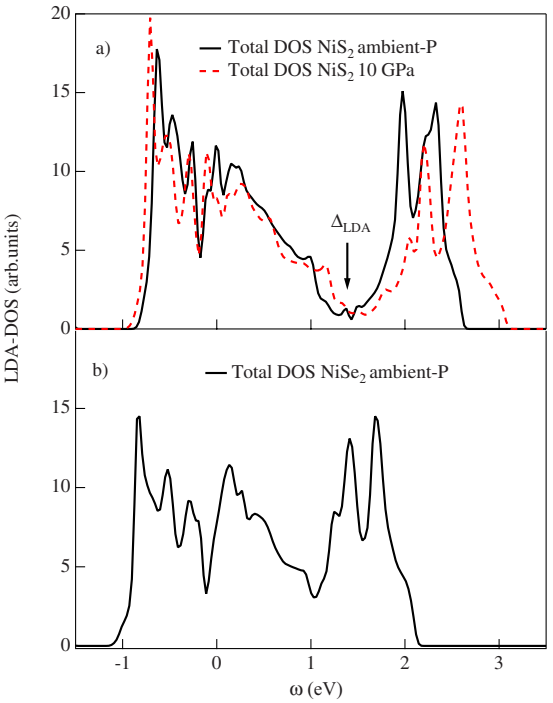

FIG. 3. (Color online) (a) Total LDA-DOS for NiS_2. Solid line represent the DOS at ambient P, dashed lines at 10 GPa. (b) Total LDA-DOS for the $NiSe_2$ compound. In the case of NiS_2, the 10 GPa DOS can be rescaled by a factor 0.88 on that at ambient P, resulting in an increase in W_{e_g}/U, keeping W_{e_g}/Δ_{LDA} fixed. In contrast, Se substitution results in a decrease in W_{e_g}/U and an increase in W_{e_g}/Δ_{LDA} due to the shrinking of the charge-transfer gap Δ_{LDA}.

Let us now turn back to the optical experiment in Fig. 2. Deep inside the metallic phase, we can expect correlations to be weak and LDA to give the proper answer. Within LDA we

calculated the "square plasma frequency," which is defined as the average over the Fermi Surface of the squared velocities. In Figs. 2(b) and 2(c) we compare the square plasma frequency to the experimental SW. Because of the different changes in the band structure under pressure and upon Se alloying, LDA gives nonmonotonic behavior and very different slopes in agreement with experiment, see Figs. 2(b) and 2(c). For the insulating NiS_2 compound and close to the phase transition, electronic correlations are not negligible and we performed LDA+DMFT (Refs. 34 and 35) calculations. To this end, the NMTO band structure was downfolded to effective Ni e_g states and the correlations in these two orbitals were treated by means of DMFT. For $U>3J$ (U being the intraorbital Coulomb interaction between the Ni e_g states and J the Hund coupling), the two e_g-orbitals split and a gap opens for NiS_2. This insulating LDA+DMFT solution results in a very strong suppression of the square plasma frequency (as well as of the SW) as indicated by the vertical arrow in Figs. 2(b) and 2(c).

Besides important similarities between the P- and Se-dependent phase diagrams,[4,22] the present optical study reveals that a simple linear scaling between P and x, as that indicated by transport, does not hold at finite frequencies. This suggests that the two MITs rely on distinct microscopic mechanisms. These mechanisms can be understood theoretically in terms of the two fundamental parameters for the MIT in a CT insulator: Under pressure, $W_{e_g}/\Delta_{\mathrm{LDA}}=\mathrm{const}$ and W_{e_g}/U increases, triggering the MIT; in contrast upon alloying Se, the increase in $W_{e_g}/\Delta_{\mathrm{LDA}}$ is responsible for the MIT whereas W_{e_g}/U even decreases. This makes $NiS_{2-x}Se_x$ under pressure an ideal system for the study of the MIT in a CT strongly correlated system.

The authors acknowledge L. Baldassarre and E. Arcangeletti for preliminary optical measurements and M. Polentarutti for x-ray characterization of the NiS_2 compound. This work was financially supported by the Austrian Fonds zur Förderung der wissenschaftlichen Forschung.

[1] M. Imada *et al.*, Rev. Mod. Phys. **70**, 1039 (1998).
[2] J. Zaanen, G. A. Sawatzky, and J. W. Allen, Phys. Rev. Lett. **55**, 418 (1985).
[3] N. F. Mott, Proc. Phys. Soc., London, Sect. A **62**, 416 (1949).
[4] S. Miyasaka *et al.*, J. Phys. Soc. Jpn. **69**, 3166 (2000).
[5] P. G. Niklowitz, M. Steiner, G. Lonzarich, D. Braithwaite, G. Knebel, J. Flouquet, and J. Wilson, arXiv:cond-mat/0610166 (unpublished).
[6] M. J. Rozenberg, G. Kotliar, H. Kajueter, G. A. Thomas, D. H. Rapkine, J. M. Honig, and P. Metcalf, Phys. Rev. Lett. **75**, 105 (1995).
[7] L. Baldassarre *et al.*, Phys. Rev. B **77**, 113107 (2008).
[8] G. Kotliar *et al.*, Rev. Mod. Phys. **78**, 865 (2006).
[9] Y. Okimoto, T. Katsufuji, Y. Okada, T. Arima, and Y. Tokura, Phys. Rev. B **51**, 9581 (1995).
[10] A. Congeduti *et al.*, Phys. Rev. B **63**, 184410 (2001).
[11] P. Postorino, A. Congeduti, P. Dore, A. Sacchetti, F. Gorelli, L. Ulivi, A. Kumar, and D. D. Sarma, Phys. Rev. Lett. **91**, 175501 (2003).
[12] A. Pashkin, M. Dressel, and C. A. Kuntscher, Phys. Rev. B **74**, 165118 (2006).
[13] D. D. Sarma *et al.*, Phys. Rev. B **67**, 155112 (2003); D. D. Sarma, M. Pedio, M. Capozi, A. Girycki, N. Chandrasekharan, N. Shanthi, S. R. Krishnakumar, C. Ottaviani, C. Quaresima, and P. Perfetti, *ibid.* **57**, 6984 (1998).
[14] Due to the cubic $NiS_{2-x}Se_x$ structure, IR data on high-density pellets are not affected by anisotropic effects.
[15] A. Sacchetti, E. Arcangeletti, A. Perucchi, L. Baldassarre, P. Postorino, S. Lupi, N. Ru, I. R. Fisher, and L. Degiorgi, Phys. Rev. Lett. **98**, 026401 (2007).
[16] S. Lupi *et al.*, J. Opt. Soc. Am. B **24**, 959 (2007).
[17] L. Baldassarre, A. Perucchi, E. Arcangeletti, D. Nicoletti, D. Di Castro, P. Postorino, V. A. Sidorov, and S. Lupi, Phys. Rev. B **75**, 245108 (2007).
[18] E. Arcangeletti, L. Baldassarre, D. Di Castro, S. Lupi, L. Malavasi, C. Marini, A. Perucchi, and P. Postorino, Phys. Rev. Lett. **98**, 196406 (2007).
[19] F. Wooten, *Optical Properties of Solids* (Academic, New York, 1972).
[20] M. Dressel and G. Grüner, *Electrodynamics of Solids* (Cambridge University Press, Cambridge, England, 2002).
[21] R. L. Kautz *et al.*, Phys. Rev. B **6**, 2078 (1972).
[22] A. Fujimori, Phys. Status Solidi B **233**, 47 (2001).
[23] P. Kwizera, M. S. Dresselhaus, and D. Adler, Phys. Rev. B **21**, 2328 (1980).
[24] T. Fujii *et al.*, Mineral. J. **13**, 448 (1987).
[25] X. Yao, Y. K. Kuo, D. K. Powell, J. W. Brill, and J. M. Honig, Phys. Rev. B **56**, 7129 (1997).
[26] F. D. Murnaghan, Proc. Natl. Acad. Sci. U.S.A. **30**, 244 (1944).
[27] S. Jiuxun *et al.*, J. Phys. Chem. Solids **66**, 773 (2005).
[28] Concerning the LDA analysis, $a(P)$ values were calculated using the TB-LMTO plus LDA method and the so-called *force theorem*, that is, the change in the total energy under uniform compression, (see, e.g., Ref. 29).
[29] A. R. Mackintosh and O. K. Andersen, in *Electrons at the Fermi Surface*, edited by M. Springford(Cambridge University Press, Cambridge, 1980), p. 149.
[30] O. K. Andersen and O. Jepsen, Phys. Rev. Lett. **53**, 2571 (1984).
[31] O. K. Andersen *et al.*, *Electronic Structure and Physical Properties of Solids: The Uses of the LMTO method*, edited by H. Dreysse, Lecture Notes in Physics (Springer, New York, 2000); O. K. Andersen and T. Saha-Dasgupta, Phys. Rev. B, **62**, R16219 (2000); E. Zurek, O. Jepsen, and O. K. Andersen, ChemPhysChem **6**, 1934 (2005).
[32] K. Schwarz, P. Blaha, and G. K. H. Madsen, Comput. Phys. Commun. **147**, 71 (2002).
[33] A. Y. Matsuura, Z. X. Shen, D. S. Dessau, C. H. Park, T. Thio, J. W. Bennett, and O. Jepsen, Phys. Rev. B **53**, R7584 (1996).
[34] The Hirsch-Fye quantum Monte Carlo simulation has been used for solving the DMFT equations.
[35] V. I. Anisimov *et al.*, J. Phys.: Condens. Matter **9**, 7359 (1997); A. I. Lichtenstein and M. I. Katsnelson, Phys. Rev. B **57**, 6884 (1998); K. Held, Adv. Phys. **56**, 829 (2007).